J. Fluid Mech. (2021), *vol*. 907, A10. © The Author(s), 2020.
Published by Cambridge University Press
doi:10.1017/jfm.2020.803

The corotating hollow vortex pair: steady merger and break-up via a topological singularity

R. B. Nelson[1],†, **V. S. Krishnamurthy**[2] **and D. G. Crowdy**[3]

[1]Department of Earth Science and Engineering, Imperial College London, London SW7 2AZ, UK

[2]Faculty of Mathematics, University of Vienna, Oskar-Morgenstern-Platz 1, 1090 Vienna, Austria

[3]Department of Mathematics, Imperial College London, London SW7 2AZ, UK

(Received 27 May 2020; revised 14 September 2020; accepted 16 September 2020)

The shapes of two steadily rotating, equal circulation, two-dimensional hollow vortices are determined and their properties examined. By means of a numerical scheme that accounts for the doubly connected nature of the fluid domain, it is shown that a one-parameter family of solutions exists that is a continuation of a corotating point-vortex pair. With $b = 2$ set as the distance between the vortex centroids, we find that each vortex reaches a maximum possible area of 0.796 corresponding to $a/b = 0.260$ where a is a measure of the vortex core radius proposed by Meunier *et al.* (*Phys. Fluids*, vol. 14, 2002, pp. 2757–2766). Results are compared to those of a previous study by Saffman & Szeto (*Phys. Fluids*, vol. 23, 1980, pp. 2339–2342) in which two corotating patches of uniform vorticity are considered in place of the hollow vortices studied here. The general behaviour of the two systems is seen to be similar but some differences are highlighted, especially when the vortices become close to touching due to the accumulation of vorticity in thin extended fingers emanating from each of the vortices. The numerical scheme captures the family of equilibria very close to a critical configuration where these fingers tend to touch at the centre of rotation corresponding to $a/b \approx 0.283$. By a simple adaptation of the numerical scheme to compute 2-fold rotationally symmetric equilibria for a single rotating hollow vortex we then show that its limiting configuration is one where a thin waist forms leading to two separate parts of its single boundary drawing close together. We give evidence that the limit of this single vortex configuration coincides with the limit of the two-vortex configuration. The limiting configuration itself turns out not to be physically admissible, leading to what we refer to as a topological singularity since no physical quantities blow up, indeed they appear to be continuous as the limiting state is approached from the two topologically distinct directions.

Key words: vortex dynamics, vortex interactions

1. Introduction

The study of two interacting like-signed two-dimensional vortices, or a 'vortex pair', is an important basic problem in fluid mechanics and is the topic of a recent review (Leweke, Dizés & Williamson 2016). When each vortex is modelled as a point vortex of circulation Γ the configuration rotates with constant angular velocity $\Gamma/(4\pi r^2)$ about the origin if the

† Email address for correspondence: rnelson@ic.ac.uk

vortices are fixed at $(\pm r, 0)$ in a corotating frame of reference. In reality it is known that vortices with a finite core size remain in steady rotation or coalesce ('merge') depending on how large they are compared to the separation of their vortex centroids (Dritschel 1985; Melander, Zabusky & McWilliams 1988; Meunier *et al.* 2002; Leweke *et al.* 2016). There are many studies linking the question of dynamical vortex merger with the loss of existence of steadily rotating equilibria (Meunier *et al.* 2002; Leweke *et al.* 2016) making the study of corotating pairs of particular significance.

Finite-size vortices are most commonly modelled in the theoretical literature using the vortex patch model where the vorticity is assumed to be non-zero and uniform in finite bounded regions of fluid. Saffman & Szeto (1980) computed the shapes of two steadily rotating vortex patches. They were interested in understanding the continual coalescence of the organised or coherent structures of the turbulent mixing layer and the merging of vortices in the wakes of lifting bodies. They looked for steady corotating equilibria and found a one-parameter family of solutions that could be thought of as being grown from the point-vortex solution; they showed there is a minimum centroid separation – discussed quantitatively later in this paper – for steady rotation to be possible. They also computed equilibria beyond this minimum where the centroid separation increases and the vortices become elongated and close to touching. Saffman & Schatzman (1981) computed the structure of steady staggered streets of vortex patches numerically. Many similar studies of equilibrium vortex patch configurations are surveyed by Saffman (1992).

A much older model of distributed vorticity, dating back to the 19th century, is the hollow vortex model where a vortex is modelled as a finite-area constant pressure region having a non-zero circulation around it (Baker, Saffman & Sheffield 1976; Saffman 1992). In one of the earliest studies Pocklington (1895) found an analytical solution for two steadily translating hollow vortices of opposite circulation, a problem revisited recently in Crowdy, Llewellyn Smith & Freilich (2013) where the authors used a so-called prime function (Crowdy 2020) to rederive Pocklington's original solution in a more convenient form which, in particular, facilitated a linear stability calculation. There has been a recent resurgence of interest in the hollow vortex model: other studies include Tanveer (1986), Telib & Zannetti (2011) and Llewellyn Smith & Crowdy (2012) and a hollow vortex analogue of von Kármán's staggered point-vortex street (Crowdy & Green 2011); the last two studies are given in the form of analytical solutions. In a natural extension of the analytical solution for a steady hollow vortex in a linear strain found by Llewellyn Smith & Crowdy (2012), Zannetti, Ferlauto & Llewellyn Smith (2016) recently calculated equilibrium hollow vortices embedded in a shear flow (analytical solutions do not appear to be available in this case). Other recent related work on steady vortex structures involves vortices of Sadovskii type comprising a vortex patch with a vortex sheet on its boundary rather than the usual vortex jump (Freilich & Llewellyn Smith 2017).

This proliferation of fundamental theoretical results based on the hollow vortex model is missing one basic flow scenario: that of a corotating pair of hollow vortices. This case is studied here; the shapes of two like-signed hollow vortices in steady rotation are calculated and discussed. After introducing the problem in § 2, and elucidating how we define the vortex centroid and some other relevant quantities, a convenient numerical formulation is presented in §§ 3–4 that facilitates ready numerical calculation of the two corotating hollow vortices. The scheme is similar in spirit to that used in Zannetti *et al.* (2016), but since the flow domain is now doubly connected suitable adjustments are required. A characterisation of the solutions is given in § 5. The scheme allows us to follow a family of solutions very close to a limiting state where two thin fingers emanating from each vortex tend towards the centre of rotation and touch. To get more insight into the situation, in § 6 we examine the complementary limit of a single rotating hollow vortex

with a 2-fold rotationally symmetric perturbation from a circular hollow vortex and give evidence that it tends to the same limiting state. This result is interpreted as evidence of a topological singularity since no physical quantities blow up and indeed are continuous across the topological transition.

2. Formulation

Of interest is the identification of relative equilibria in which a pair of equal circulation hollow vortices rotate with constant angular velocity Ω about the geometrical mid-point between them. Since hollow vortices only appear to have been previously studied in steady equilibrium (e.g. Llewellyn Smith & Crowdy 2012; Zannetti *et al.* 2016) or in steadily translating configurations (Pocklington 1895; Crowdy & Green 2011) it is not immediately clear how to define a steadily rotating hollow vortex. Here, we take the arrangement to be two equal-sized finite-area regions, each with equal non-zero circulation Γ, and with interiors that are in pure solid body rotation with some angular velocity Ω about the centre point between them. In a frame of reference corotating with the vortices, the flow inside the vortices therefore vanishes and can be considered a constant pressure region.

The flow $\boldsymbol{u} = (u, v)$ is incompressible so we can introduce a streamfunction $\psi(x, y)$ such that

$$u = \frac{\partial \psi}{\partial y}, \quad v = -\frac{\partial \psi}{\partial x}. \tag{2.1a,b}$$

Exterior to the vortices the streamfunction ψ in the corotating frame satisfies

$$\nabla^2 \psi = -\omega = 2\Omega, \tag{2.2}$$

where $\omega(x, y)$ denotes the vorticity field. The irrotational flow exterior to the vortices in the fixed frame becomes a uniform vorticity -2Ω in the corotating frame. The kinematic condition that each vortex boundary is a streamline in the corotating frame, together with Bernoulli's theorem (Saffman 1992; Batchelor 2000) and the condition that the pressure is constant on the boundary of each vortex imply that

$$\boldsymbol{u} \cdot \boldsymbol{n} = 0, \quad \boldsymbol{u} \cdot \boldsymbol{t} = q, \tag{2.3a,b}$$

on each vortex boundary where $\boldsymbol{n}$ is the outward normal to the boundary and $\boldsymbol{t}$ is its tangent vector as the boundary is traversed in an anticlockwise direction. The constant q is the fluid speed on the vortex boundary. This is a free boundary problem in which both the shape of the two hollow vortices and the flow exterior to them must be determined simultaneously, along with the parameters Ω and q.

In the corotating frame it is convenient to introduce the complex variable $z = x + \mathrm{i}y$ and its complex conjugate $\bar{z} = x - \mathrm{i}y$ and to write (2.2) as

$$\frac{\partial^2 \psi}{\partial z \partial \bar{z}} = \frac{\Omega}{2}, \tag{2.4}$$

which allows integration with respect to z and $\bar{z}$

$$\psi = \frac{\Omega}{2} z\bar{z} + \mathrm{Im}[w(z)], \tag{2.5}$$

where $w(z)$ is the complex potential for an irrotational flow exterior to the vortices. It is convenient to decompose $w(z)$ as

$$w(z) = w_\Gamma(z) + h(z), \tag{2.6}$$

where $w_\Gamma(z)$ adds in the circulation Γ around the vortices and satisfies the streamline condition on their boundaries; the contribution $h(z)$, on the other hand, will have zero circulation around the two vortices.

The boundary conditions (2.3*a*,*b*) on each vortex boundary can be written in complex form as

$$u + \mathrm{i}v = q\frac{\mathrm{d}z}{\mathrm{d}s}, \tag{2.7}$$

where $\mathrm{d}z/\mathrm{d}s$ is the complex tangent and $\mathrm{d}s$ is the arclength element that increases as each vortex boundary is traversed in an anticlockwise direction. Using (2.5), we deduce that

$$u - \mathrm{i}v = 2\mathrm{i}\frac{\partial\psi}{\partial z} = \mathrm{i}\Omega\bar{z} + \frac{\mathrm{d}w}{\mathrm{d}z} \tag{2.8}$$

and hence, using (2.7), it follows that

$$\mathrm{i}\Omega\bar{z} + \frac{\mathrm{d}w}{\mathrm{d}z} = q\frac{\mathrm{d}\bar{z}}{\mathrm{d}s} \tag{2.9}$$

on the boundary of each vortex.

The total circulation Γ of each vortex is given by

$$\Gamma = q\mathcal{P} + 2\Omega\mathcal{A}, \tag{2.10}$$

where we have added the contribution from the constant tangential speed q around the vortex perimeter $\mathcal{P}$ to the uniform vorticity 2Ω over the vortex area $\mathcal{A}$. Since the circulation is defined to be

$$\Gamma = \int\int_{D_0} \tilde{\omega}(z,\bar{z})\,\mathrm{d}A, \tag{2.11}$$

where D_0 denotes, say, the vortex centred on the positive y axis and $\tilde{\omega}(z,\bar{z})$ is the vorticity distribution inside the vortex. The vorticity $\tilde{\omega}(z,\bar{z})$ can then be expressed as

$$\tilde{\omega}(z,\bar{z}) = q\delta(n) + 2\Omega, \tag{2.12}$$

where we think of an orthogonal coordinate system (s,n) for which the boundary ∂D_0 corresponds to $n = 0$ on which s corresponds to arclength around the $n = 0$ contour. The vortex centroid $z_c^{(v)}$ and the geometrical centroid z_c can be defined (Saffman 1992) by

$$\Gamma z_c^{(v)} = \int\int_{D_0} z\tilde{\omega}(z,\bar{z})\,\mathrm{d}A, \quad \mathcal{A}z_c = \int\int_{D_0} z\,\mathrm{d}A. \tag{2.13a,b}$$

It is easy to show that, for the rotating hollow vortex, $z_c^{(v)}$ and z_c are related by

$$\Gamma z_c^{(v)} = q\oint_{\partial D_0} z\,\mathrm{d}s + 2\Omega\mathcal{A}z_c, \tag{2.14}$$

from which we see, using (2.10), that when $q = 0$ the vortex centroid coincides with the geometrical centroid but not otherwise.

For use later we will also define the quantity

$$J_0 \equiv \int\int_{D_0} |z|^2 \tilde{\omega}(z,\bar{z})\,\mathrm{d}A = \oint_{\partial D_0} q|z|^2\,\mathrm{d}s + 2\Omega \int\int_{D_0} |z|^2\,\mathrm{d}A. \tag{2.15}$$

By Stokes' theorem we can write

$$\int\int_{D_0} |z|^2\,\mathrm{d}A = \frac{1}{2\mathrm{i}} \oint_{\partial D_0} \frac{z\bar{z}^2}{2}\mathrm{d}z, \tag{2.16}$$

which means that J_0 can be determined by evaluating a contour integral

$$J_0 = \oint_{\partial D_0} q|z|^2\,\mathrm{d}s - \frac{\mathrm{i}\Omega}{2} \oint_{\partial D_0} z\bar{z}^2\mathrm{d}z. \tag{2.17}$$

Meunier *et al.* (2002) introduced a measure of the size of a vortex, to be considered later, based on the quantity J defined to be

$$J = \int\int_{D_0} |z - z_c^{(v)}|^2 \tilde{\omega}(z,\bar{z})\,\mathrm{d}A. \tag{2.18}$$

After some algebra, and on use of (2.11) and (2.13*a*,*b*), we can establish that

$$J = J_0 - |z_c^{(v)}|^2 \Gamma. \tag{2.19}$$

3. Conformal mapping

Given the doubly connected nature of the fluid region we will deploy a conformal mapping method from a parametric annulus, $\rho < |\zeta| < 1$; see figure 1 where we see that the unit circle $|\zeta| = 1$ is denoted by C_0 and the circle $|\zeta| = \rho$ by C_1. Points in the z and ζ-planes are related via the conformal mapping $z = Z(\zeta)$ which must be determined; it will give the shape of the vortices. We take one of the vortices to lie in the upper-half z-plane, the other being a reflection of it in the real axis. For such a configuration the conformal mapping can be written as

$$Z(\zeta) = \mathrm{i}d\left[\left(\frac{\zeta - \sqrt{\rho}}{\zeta + \sqrt{\rho}}\right) + \sum_{n=1}^{\infty} a_n\zeta^n - a_n\left(\frac{\rho}{\zeta}\right)^n\right], \tag{3.1}$$

where $d \in \mathbb{R}$ is a scaling parameter and the coefficients $\{a_n \in \mathbb{R}\}$ are to be found. Under (3.1) the pre-image of the point at infinity in the co-rotating plane is $\zeta = -\sqrt{\rho}$ and the pre-image of the origin is $\zeta = \sqrt{\rho}$. It is also easily checked that

$$Z(\rho/\zeta) = -Z(\zeta), \tag{3.2}$$

which guarantees that the vortices are rotations of each other through 180°. It follows from (3.1) that

$$\zeta Z'(\zeta) = \mathrm{i}d\left[\frac{2\sqrt{\rho}\zeta}{(\zeta + \sqrt{\rho})^2} + \sum_{n=1}^{\infty} na_n\zeta^n + na_n\left(\frac{\rho}{\zeta}\right)^n\right], \tag{3.3}$$

where primes are used to denote differentiation with respect to the argument of the function. An integral expression for a_n in terms of $\zeta Z'(\zeta)$ follows by equating residues,

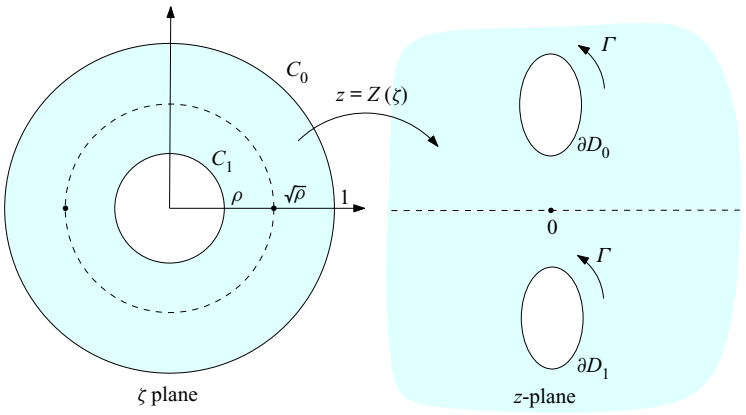

FIGURE 1. Conformal mapping from a concentric annulus $\rho < |\zeta| < 1$ to the fluid region exterior to two hollow vortices in the corotating z-plane where the vortices are stationary.

namely,

$$a_n = -\frac{1}{2\pi i n}\oint_{C_0}\left[\frac{i\zeta Z'(\zeta)}{d} + \frac{2\sqrt{\rho}\zeta}{(\zeta+\sqrt{\rho})^2}\right]\frac{d\zeta}{\zeta^{n+1}}, \quad n \geq 1, \tag{3.4}$$

which will be useful later.

Armed with the conformal mapping function the following composed functions can be introduced:

$$W_\Gamma(\zeta) \equiv w_\Gamma(Z(\zeta)), \quad H(\zeta) \equiv h(Z(\zeta)). \tag{3.5a,b}$$

The form of $W_\Gamma(\zeta)$ follows from a general calculus for finding complex potentials associated with ideal flows in multiply connected domains described in Crowdy (2010, 2020) and is

$$W_\Gamma(\zeta) = -\frac{i\Gamma}{2\pi}\log\zeta + \frac{i\Gamma}{\pi}\log\left(\frac{P(-\zeta/\sqrt{\rho},\rho)}{|\sqrt{\rho}|P(-\zeta\sqrt{\rho},\rho)}\right), \tag{3.6}$$

where

$$P(\zeta,\rho) = \sum_{n=-\infty}^{\infty}(-1)^n\rho^{n(n-1)}\zeta^n. \tag{3.7}$$

The function $P(\zeta,\rho)$ defined by this rapidly convergent sum is essentially the so-called prime function for the annulus (Crowdy 2020). It is the same function used by Crowdy *et al.* (2013) in their rederivation of Pocklington's cotravelling hollow vortex pair. Actually, only the quantity $\zeta W_\Gamma'(\zeta)$ will be needed in what follows and this can be written as

$$\zeta W_\Gamma'(\zeta) = \frac{i\Gamma}{2\pi}[2K(-\zeta/\sqrt{\rho},\rho) - 2K(-\zeta\sqrt{\rho},\rho) - 1], \tag{3.8}$$

where

$$K(\zeta,\rho) \equiv \frac{\zeta}{P(\zeta,\rho)}\frac{\partial}{\partial\zeta}P(\zeta,\rho). \tag{3.9}$$

4. Solving for $H(\zeta)$ and $Z(\zeta)$

While $W_\Gamma(\zeta)$ is known, the function $H(\zeta)$ and the mapping $Z(\zeta)$ remain to be determined from the boundary conditions (2.8). Multiplication of (2.8) by $\mathrm{d}z/\mathrm{d}s$, and use of (2.6), yields

$$\frac{\mathrm{d}z}{\mathrm{d}s}\frac{\mathrm{d}h}{\mathrm{d}z} = q - \mathrm{i}\Omega\bar{z}\frac{\mathrm{d}z}{\mathrm{d}s} - \frac{\mathrm{d}z}{\mathrm{d}s}\frac{\mathrm{d}w_\Gamma}{\mathrm{d}z} \tag{4.1}$$

on each vortex boundary. Noting, from the chain rule and (3.5*a*,*b*), that

$$\frac{\mathrm{d}h}{\mathrm{d}z} = \frac{H'(\zeta)}{Z'(\zeta)}, \quad \frac{\mathrm{d}w_\Gamma}{\mathrm{d}z} = \frac{W_\Gamma'(\zeta)}{Z'(\zeta)}, \tag{4.2a,b}$$

and the fact that

$$\frac{\mathrm{d}z}{\mathrm{d}s} = \begin{cases} -\dfrac{\mathrm{i}\zeta Z'(\zeta)}{|Z'(\zeta)|}, & \zeta \in C_0, \\ +\dfrac{\mathrm{i}\zeta Z'(\zeta)}{\rho|Z'(\zeta)|}, & \zeta \in C_1, \end{cases} \tag{4.3}$$

where the choice of sign in these expressions ensures that $\mathrm{d}s$ increases as the boundary curve is traversed in the anticlockwise direction, (4.1) can be written as

$$\mathrm{i}\zeta H'(\zeta) = \begin{cases} -q|Z'(\zeta)| + \Omega\overline{Z(\zeta)}\zeta Z'(\zeta) - \mathrm{i}\zeta W_\Gamma'(\zeta), & \zeta \in C_0, \\ q\rho|Z'(\zeta)| + \Omega\overline{Z(\zeta)}\zeta Z'(\zeta) - \mathrm{i}\zeta W_\Gamma'(\zeta), & \zeta \in C_1. \end{cases} \tag{4.4}$$

The real and imaginary parts of these conditions will be needed in formulating the solution procedure.

First, on taking the imaginary part of (4.4) it is found that

$$\mathrm{Im}[\mathrm{i}\zeta H'(\zeta)] = \mathrm{Im}[\Omega\overline{Z(\zeta)}\zeta Z'(\zeta)] - \mathrm{Im}[\mathrm{i}\zeta W_\Gamma'(\zeta)], \quad \zeta \in C_0, C_1, \tag{4.5}$$

or, equivalently,

$$\mathrm{Re}[\zeta H'(\zeta)] = R_0(\zeta), \quad \zeta \in C_0, C_1, \tag{4.6}$$

where

$$R_0(\zeta) = \mathrm{Im}[\Omega\overline{Z(\zeta)}\zeta Z'(\zeta)] - \mathrm{Re}[\zeta W_\Gamma'(\zeta)]. \tag{4.7}$$

Therefore, (4.6) is a specification, on the two boundaries of the annulus, of the real part of a function $\zeta H'(\zeta)$ known to be analytic and single valued in the annulus. If those real parts are known this is a well-known problem in complex analysis: it is the modified Schwarz problem in the annulus (Crowdy 2008, 2020). The solution is furnished, up to a purely imaginary constant, by the integral formula

$$\zeta H'(\zeta) = I_1(\zeta) + \mathrm{i}c_1, \tag{4.8}$$

where $c_1 \in \mathbb{R}$ is a constant and

$$I_1(\zeta) \equiv \frac{1}{2\pi\mathrm{i}}\oint_{C_0} R_0(\zeta')[2K(\zeta'/\zeta,\rho) - 1]\frac{\mathrm{d}\zeta'}{\zeta'} - \frac{1}{2\pi\mathrm{i}}\oint_{C_1} R_0(\zeta')[2K(\zeta'/\zeta,\rho)]\frac{\mathrm{d}\zeta'}{\zeta'}, \tag{4.9}$$

where K is the function introduced in (3.9) (Crowdy 2008, 2020). It must be true that $c_1 = 0$ in order to avoid a term $\mathrm{i}c_1 \log\zeta$ in $H(\zeta)$ which would alter the circulation of the vortices

which has already been fixed by the choice of the contribution $W_\Gamma(\zeta)$ to the complex potential. While the integral formula (4.9) is explicit, it is often more convenient to use another method based on equating coefficients in a Laurent series representation of the unknown function; this method is described in appendix D of Crowdy & Krishnamurthy (2018); see also Crowdy (2020). Either way, in order for a solution for $\zeta H'(\zeta)$ to exist, a solvability condition must be satisfied and this takes the form (Crowdy 2008, 2020)

$$\oint_{C_0} R_0(\zeta)\frac{\mathrm{d}\zeta}{\zeta} - \oint_{C_1} R_0(\zeta)\frac{\mathrm{d}\zeta}{\zeta} = 0. \tag{4.10}$$

Since $\mathrm{Im}[W_\Gamma(\zeta)] = 0$ on both C_0 and C_1 then, for example, on C_0,

$$W_\Gamma(\zeta) = \overline{W_\Gamma}(1/\zeta) \tag{4.11}$$

and hence, on differentiation with respect to ζ,

$$W_\Gamma'(\zeta) = -\frac{1}{\zeta^2}\overline{W_\Gamma}'(1/\zeta) \quad \text{or} \quad \mathrm{Re}[\zeta W_\Gamma'(\zeta)] = 0, \quad \zeta \in C_0, \tag{4.12}$$

with the same deduction holding for $\zeta \in C_1$. Thus, by virtue of our special choice of $W_\Gamma(\zeta)$, the solvability condition (4.10) reduces, using (4.7), to

$$\oint_{C_0} \mathrm{Im}\left[\overline{Z(\zeta)}\zeta Z'(\zeta)\right]\frac{\mathrm{d}\zeta}{\zeta} - \oint_{C_1} \mathrm{Im}\left[\overline{Z(\zeta)}\zeta Z'(\zeta)\right]\frac{\mathrm{d}\zeta}{\zeta} = 0. \tag{4.13}$$

However, the first term on the left-hand side is

$$\begin{aligned}\oint_{C_0} \mathrm{Im}\left[\overline{Z(\zeta)}\zeta Z'(\zeta)\right]\frac{\mathrm{d}\zeta}{\zeta} &= \frac{1}{2\mathrm{i}}\oint_{C_0}\frac{\mathrm{d}\zeta}{\zeta}(\bar{Z}(\zeta^{-1})\zeta Z'(\zeta) - Z(\zeta)\zeta^{-1}\bar{Z}'(\zeta^{-1})) \\ &= \frac{1}{2\mathrm{i}}\oint_{C_0}\bar{Z}\,\mathrm{d}Z + Z\,\mathrm{d}\bar{Z} = \frac{1}{2\mathrm{i}}\oint_{C_0}\mathrm{d}(Z\bar{Z}) = 0,\end{aligned} \tag{4.14}$$

provided $Z(\zeta)$ is a single-valued function around C_0, as must be the case if it is to represent the required conformal mapping; this single-valuedness requirement on the mapping function will be enforced explicitly later. A similar result holds for the second term on the left hand side of (4.13). Thus the solvability condition (4.10) is satisfied if $Z(\zeta)$ is single valued in the annulus. If the solvability condition is satisfied the solution (4.8) of the modified Schwarz problem for $\zeta H'(\zeta)$ exists.

Next, the real part of (4.4) leads to

$$|\zeta Z'(\zeta)| = \begin{cases} S_0(\zeta), & \zeta \in C_0, \\ -S_0(\zeta), & \zeta \in C_1, \end{cases} \tag{4.15}$$

where

$$S_0(\zeta) = \frac{1}{q}\left[\mathrm{Re}[\Omega\overline{Z(\zeta)}\zeta Z'(\zeta)] + \mathrm{Im}[\zeta W_\Gamma'(\zeta) + \zeta H'(\zeta)]\right]. \tag{4.16}$$

Since $\zeta Z'(\zeta)$ must not vanish in the annulus if $Z(\zeta)$ is a univalent conformal mapping from the annulus to the fluid region then, from (3.3), the function defined by

$$F(\zeta) \equiv \log(\zeta Z'(\zeta)) + \log\left[\frac{(\zeta + \sqrt{\rho})^2}{\zeta}\right] \tag{4.17}$$

is analytic and single valued in the annulus because, on inspection of (3.3), the logarithmic singularities of the two functions on the right-hand side at $\zeta = 0, -\sqrt{\rho}$ cancel out.

Moreover, on use of (4.15),

$$\mathrm{Re}[F(\zeta)] = \begin{cases} T_0(\zeta), & \zeta \in C_0, \\ T_1(\zeta), & \zeta \in C_1, \end{cases} \tag{4.18}$$

where

$$T_0(\zeta) \equiv \log(S_0(\zeta)) + \log\left|\frac{(\zeta+\sqrt{\rho})^2}{\zeta}\right|, \quad T_1(\zeta) \equiv \log(-S_0(\zeta)) + \log\left|\frac{(\zeta+\sqrt{\rho})^2}{\zeta}\right|. \tag{4.19a,b}$$

Consequently, (4.18) is a second modified Schwarz problem in the annulus, this time for the single-valued analytic function $F(\zeta)$. The solvability condition associated with this second modified Schwarz problem is

$$\int_{C_0} \frac{\mathrm{d}\zeta}{\zeta} T_0(\zeta) = \int_{C_1} \frac{\mathrm{d}\zeta}{\zeta} T_1(\zeta). \tag{4.20}$$

It can be demonstrated, using arguments akin to those used for the first modified Schwarz problem, that this solvability condition is satisfied if the mapping function is single valued and satisfies the symmetry condition (3.2). Thus it has a representation

$$F(\zeta) = I_2(\zeta) + \mathrm{i}c_2, \tag{4.21}$$

where

$$I_2(\zeta) = \frac{1}{2\pi\mathrm{i}} \oint_{C_0} T_0(\zeta')[2K(\zeta'/\zeta, \rho) - 1]\frac{\mathrm{d}\zeta'}{\zeta'} - \frac{1}{2\pi\mathrm{i}} \oint_{C_1} T_0(\zeta')[2K(\zeta'/\zeta, \rho)]\frac{\mathrm{d}\zeta'}{\zeta'}. \tag{4.22}$$

From (3.3) it is necessary that

$$\mathrm{e}^{F(\zeta)} = (\zeta+\sqrt{\rho})^2 Z'(\zeta) \to 2\sqrt{\rho}d\mathrm{i} \tag{4.23}$$

as $\zeta \to -\sqrt{\rho}$ which determines c_2 according to

$$\mathrm{e}^{F(-\sqrt{\rho})} = \exp(I_2(-\sqrt{\rho}) + \mathrm{i}c_2) = 2\sqrt{\rho}d\mathrm{i}, \quad \text{or} \quad \mathrm{e}^{\mathrm{i}c_2} = 2\sqrt{\rho}d\mathrm{i}\,\mathrm{e}^{-I_2(-\sqrt{\rho})}. \tag{4.24}$$

This means that

$$Z'(\zeta) = 2\sqrt{\rho}d\mathrm{i}\frac{\exp(I_2(\zeta) - I_2(-\sqrt{\rho}))}{(\zeta+\sqrt{\rho})^2}. \tag{4.25}$$

In order that $Z(\zeta)$ has no logarithmic term at $\zeta = -\sqrt{\rho}$ it must be true that

$$I_2'(-\sqrt{\rho}) = 0. \tag{4.26}$$

It should be emphasised that the two modified Schwarz problems just described are coupled and need to be solved simultaneously.

4.1. *Solution procedure*

The time scale of the flow is fixed by setting $\Gamma = 1$. Since the problem is nonlinear an iterative scheme (Newton's method) is appropriate. The Laurent series in (3.1) is truncated to include N non-zero real coefficients $\{a_n | n = 1, \ldots, N\}$ which are N quantities to be found. All the results to follow, including the near-critical configurations, have been obtained with $N = 64$. Three other unknowns are d, Ω and q giving a total of $N + 3$ real unknowns. The equations to determine these are as follows.

The length scale for the problem is set by specifying the vortex centroids to be

$$z_c^{(v)} = \pm \mathrm{i}, \tag{4.27}$$

which, by the symmetry encoded in the formulation, constitutes a single real equation for the location on the y axis of the vortex centroid of the upper vortex. Condition (2.10) relating Γ, q and Ω must be enforced, as must the condition for the single valuedness of the mapping function,

$$\oint_{C_0} \mathrm{d}Z = 0, \tag{4.28}$$

which, again by symmetry, is a single real equation and guarantees that the conformal mapping is single valued around both vortices. To these three equations N additional equations are added as follows: given an initial guess for d, Ω, q and $\{a_n | n = 1, \ldots, N\}$ we have an initial guess for the mapping $Z(\zeta)$ and the modified Schwarz problem for $\zeta H'(\zeta)$ can be solved (we established earlier that (4.28) is the solvability condition for that problem) and that function is needed as data in the second modified Schwarz problem for $F(\zeta)$, which can then also be solved. Given $F(\zeta)$, and hence $I_2(\zeta)$ from (4.21), (4.25) provides an expression for $Z'(\zeta)$. This can be substituted into (3.4) for $n = 1, \ldots, N$ to provide N consistency conditions that must be satisfied by the coefficients in the solution representation. Together these are $N + 3$ nonlinear equations for the $N + 3$ unknowns.

The parameter ρ is used to parametrise the solution class and to serve as a continuation parameter. For small near-circular vortices with vortex centroids at $\pm\mathrm{i}$ and radius $\epsilon \ll 1$ it is expected that

$$a_n = 0 \ (n \geq 1), \quad 1 = \Gamma \approx 2\pi\epsilon q + 2\Omega\pi\epsilon^2, \quad \Omega \approx \Omega_0 \equiv \frac{\Gamma}{4\pi} = \frac{1}{4\pi}, \tag{4.29a–c}$$

where Ω_0 is the rotation rate of a pair of corotating point vortices at this separation. By analysis of the mapping (3.1), when all the coefficients $\{a_n | n = 1, \ldots, N\}$ vanish, it can be shown that the solution for two near-circular vortices corresponds to

$$\rho = \left(\frac{1 - \sqrt{1 - \epsilon^2}}{\epsilon} \right)^2 \approx \frac{\epsilon^2}{4}, \tag{4.30}$$

which will be close to zero. In the continuation procedure ρ is gradually increased and the values of $\{a_n\}$, d, Ω and q from the previous solution used as initial guesses for the next iteration. Provided steps in ρ are sufficiently small, except near critical configurations, good convergence can be expected. The algorithm is summarised as follows:

(i) Pick a small value of ϵ and find the corresponding ρ from (4.30). Then initialise the $N + 3$ parameters d, Ω, q and the coefficients $\{a_n | n \geq 1\}$ according to (4.29*a–c*).
(ii) Use Newton's method to solve the $N + 3$ nonlinear equations described above.

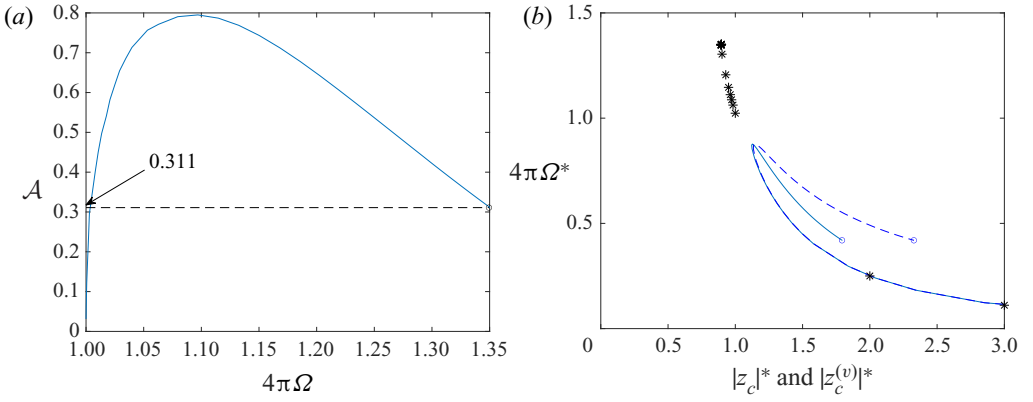

FIGURE 2. (*a*) Graph of $\Omega/\Omega_0 = 4\pi\Omega$ against $\mathcal{A}$ with the area of the critical configuration indicated. (*b*) Graph of $4\pi\Omega^*$ against the (two possible) centroid locations for the hollow vortices with normalisation $\Gamma^* = 1, \mathcal{A}^* = 1$. The solid and dashed lines represent the vortex and geometrical centroids, respectively; asterisks are for the vortex patch case (where vortex and geometrical centroids are equivalent). Vortex patch results are from table 1 of Saffman & Szeto (1980).

ρ	$\mathcal{A}$	$4\pi\Omega$	q	a/b	ρ	$\mathcal{A}$	$4\pi\Omega$	q	a/b
0.010	0.123	1.000	0.788	0.098	0.250	0.420	1.301	0.233	0.282
0.050	0.541	1.018	0.346	0.205	0.300	0.355	1.330	0.235	0.282
0.106*	0.795*	1.090*	0.249*	0.260*	0.350	0.326	1.343	0.236	0.283
0.150	0.712	1.168	0.232	0.274	0.400	0.315	1.349	0.236	0.283
0.200	0.542	1.248	0.231	0.280	0.415†	0.313†	1.350†	0.236†	0.283†

TABLE 1. Numerical values of $\mathcal{A}, 4\pi\Omega, q$ and a/b for different values of ρ. Values annotated with an asterisk correspond to the maximum area solution shown in figure 4, whereas those annotated with a dagger are for the near-critical configuration shown in figure 5.

(iii) Once the Newton iteration has converged, record all parameter values and compute $\mathcal{A}, \mathcal{P}, a/b$ for the associated vortex equilibrium (the quantity a/b is defined in § 5).
(iv) Increase ρ by a small amount and go to step (ii).

The values of $\mathcal{A}$ and $\mathcal{P}$ are calculated *a posteriori* from knowledge of the conformal mapping function. Condition (4.26) is not explicitly enforced by our solution procedure but it is verified to hold, also *a posteriori*, providing an additional consistency check on the solution.

5. Characterisation of the corotating hollow vortices

Figure 2 shows graphs of vortex area $\mathcal{A}$ against the normalised angular velocity $\Omega/\Omega_0 = 4\pi\Omega$. As ρ increases the vortex area initially increases, as does the angular velocity, until a maximum vortex area of 0.795 is reached. This occurs at $\rho \approx 0.106$ and the corresponding values of other diagnostics on this vortex configuration are recorded in table 1. For readers interested in reproducing our results this table also records this diagnostic information for a range of other ρ values. Also shown in figure 2(*b*) is a graph

of the distance $|z_c^{(v)}|$ of the vortex centroid from the centre of rotation, as well as the geometrical centroid distance $|z_c|$, as functions of the angular velocity; note that the data in this graph have been renormalised to be consistent with the different normalisation $\Gamma^* = 1, \mathcal{A}^* = 1$ used by Saffman & Szeto (1980) for corotating vortex patches (asterisks are used to reflect any quantities rewritten using this scaling). This is done to facilitate a comparison of the hollow vortex results with the vortex patch results of Saffman & Szeto (1980) whose data points are shown by asterisks in figure 2. For large separations, as expected, the systems behave in a similar manner. Marked differences occur, however, as the vortices get closer together and their shapes become more distorted from circular. In all cases these graphs exhibit a 'turnaround', where the centroids reach a minimum separation; initial signs of this turnaround were seen by Saffman & Szeto (1980) but their computations were not pushed to the same extent as here where this turnaround of the curve is seen quite distinctly. The minimum centroid separation is smaller for the vortex patch case and the corresponding angular velocity higher. For the hollow vortices the vorticity centroid and geometrical centroid remain close up until the minimum centroid separation is approached. Beyond this turnaround in the curves the hollow vortices become more elongated and the vortex centroids draw distinctly closer together compared to the geometrical centroids owing to an accumulation of circulation in the elongated tips of the vortices.

For corotating vortex patches Saffman & Szeto (1980) report the critical value of $h/R = 1.58$ where $2h$ is the centroid separation distance and πR^2 is the vortex area; the corresponding value of this quantity for the critical hollow vortex pair is $(\sqrt{0.795/\pi})^{-1} \approx 1.99$, which is clearly somewhat higher. Saffman & Szeto (1980) also mention earlier studies which had found critical values of 1.7 or 1.9 'depending on how the vortex radius was defined'. This question of how to quantify vortex size has been investigated in more detail since their work and it is perhaps more interesting to compute the value of a/b where, in this case, $b = 2$ is the distance between the vortex centroids and

$$a = \sqrt{\frac{J}{\Gamma}}, \tag{5.1}$$

is a measure of the vortex core size proposed by Meunier *et al.* (2002) where J is defined in (2.18). A graph of a/b against $\mathcal{A}$ is shown in figure 3. At the maximum value of the vortex area $\mathcal{A}$ above which equilibria no longer exist we find $a/b \approx 0.260$. The value of a/b does not itself reach a maximum at this point of maximal area, however, and it continues to increase even as the vortex area starts to decrease. The quantity a/b reaches its maximum value of $a/b \approx 0.283$ at the critical configuration where the two vortices almost touch. The values 0.260 and 0.283 are not hugely different but both values are larger than the theoretical value of 0.218 ± 0.010 proposed by Meunier *et al.* (2002) (see also the discussion in Leweke *et al.* 2016). All these discrepancies with other vortex models are likely to be attributable to the concentration of vorticity in the vortex boundaries, i.e. the contribution $q\mathcal{P}$ to the total vortex circulation, which is a feature peculiar to the hollow vortex model. Figure 3 also shows the split of the unit circulation $\Gamma = 1$ of each vortex between the two contributions $q\mathcal{P}$ and $2\Omega\mathcal{A}$ and reveals that even past the maximum area configuration most of the circulation of the vortices is held in the vorticity concentrated on their boundaries.

Figure 4 shows typical vortex shapes for $\rho = 0.05, 0.106$ and $\rho = 0.3$; the vortices for $\rho = 0.106$ correspond to the maximum area configuration. As the critical configuration is approached the two vortices extend thin 'fingers' towards the centre of rotation. The calculations suggest that the tips of these fingers draw arbitrarily close together

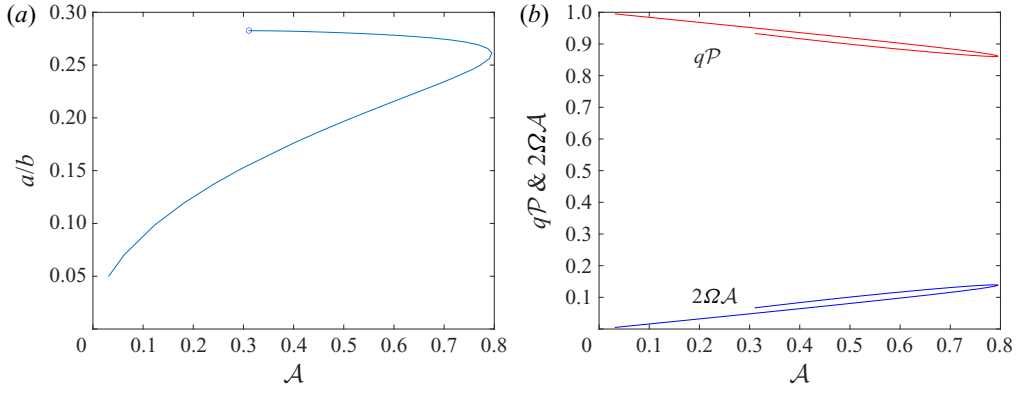

FIGURE 3. Graphs of a/b, with a defined in (5.1), $q\mathcal{P}$ and $2\Omega\mathcal{A}$, as functions of $\mathcal{A}$.

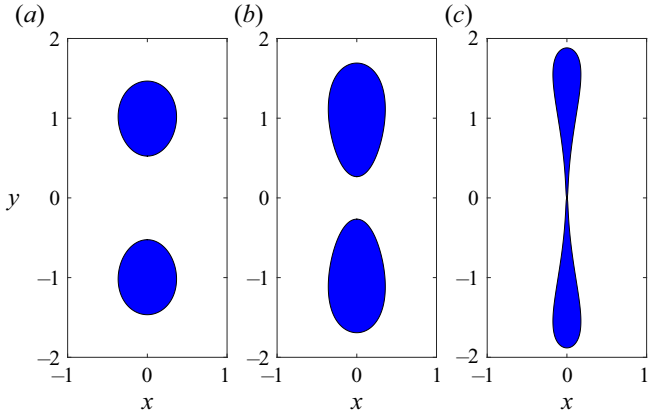

FIGURE 4. Typical equilibrium shapes of the hollow vortices in the corotating frame for $\rho = 0.05, 0.106$ and $\rho = 0.3$. The vortex centroids are fixed at $\pm$i. The case with $\rho = 0.106$ is the maximum area solution. (*a*) $\rho = 0.05$; (*b*) $\rho = 0.106$; (*c*) $\rho = 0.3$.

without blow-up of any physical quantities. The near-critical configuration, with $\rho = 0.415$, is shown in figure 5 with an inset showing the near-touching tips of the fingers protruding from each vortex towards the centre of rotation. Numerically the radius of curvature of the tip becomes so small that eventually the numerical method loses accuracy by the growth in contributions from the high-order modes and small oscillations of the vortex boundary in the vicinity of the fingers tips; with $N = 64$ modes this is found to occur, however, only after the tips of the two vortices are approximately distance 10^{-4} apart (recall that we have normalised the length scale via (4.27)).

This evidence suggests that, with higher numerical resolution, the vortices will come arbitrarily close to touching at the origin as ρ increases further. Instead of a higher-resolution numerical investigation, we adopt a different strategy to explore this possibility and ask instead about a single isolated rotating hollow vortex. No solutions for such an object have yet been reported in the literature, so we will adapt our methods and investigate this in the next section. What is known is that the only solution for an isolated non-rotating hollow vortex is a circular one (Llewellyn Smith & Crowdy 2012). But what happens if a single hollow vortex is allowed to rotate steadily? Answering this question

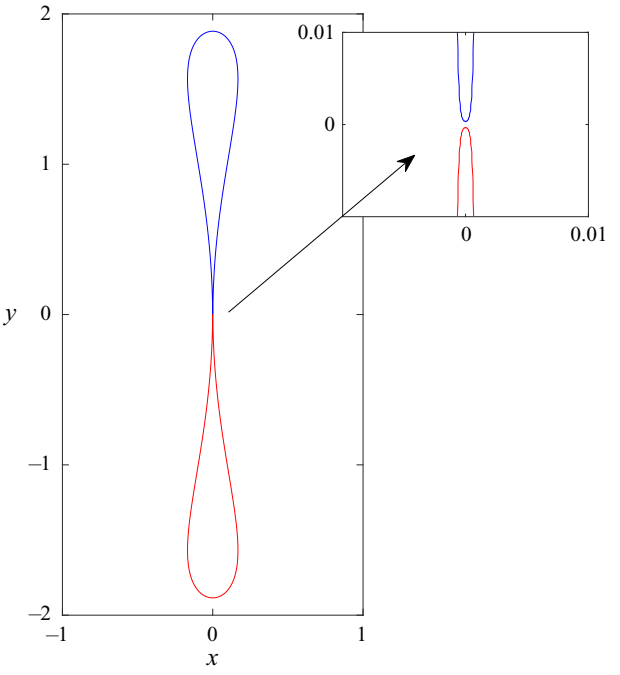

FIGURE 5. Near-critical shape of two corotating hollow vortices for $\rho = 0.415$. The inset shows a magnified view of the two near-touching 'fingers' from each vortex near the centre of rotation.

turns out to give significant insight into the limiting two-vortex configuration depicted in figure 5.

6. A single rotating hollow vortex

An advantage of conformal mapping method is that the case of a single rotating hollow vortex can be formulated immediately with only minor changes as the $\rho \to 0$ limit of the problem already formulated in the annulus. A single rotating hollow vortex is defined as a vortex of total circulation Γ rotating steadily with angular velocity Ω containing fluid in solid body rotation with this same angular velocity and with fluid of speed q on its boundary. Now the conformal mapping to the fluid region exterior to the single vortex is from the unit disc $|\zeta| < 1$. Specifically, the conformal mapping with $\zeta = 0$ mapping to infinity now takes the form

$$z = Z(\zeta) = \mathrm{i}d\left[\frac{1}{\zeta} + \sum_{n\geq 1} a_n \zeta^n\right], \tag{6.1}$$

where $\{a_n | n \geq 1\}$ are a set of real coefficients to be found. To highlight the similarities with the two-vortex problem we will use the same notation already used in that problem with the understanding that the context is now different. It is clear that

$$\zeta Z'(\zeta) = \mathrm{i}d\left[-\frac{1}{\zeta} + \sum_{n\geq 1} n a_n \zeta^n\right], \tag{6.2}$$

so that the requisite integral expression for a_n in terms of $\zeta Z'(\zeta)$ in this case is

$$a_n = -\frac{1}{2\pi d n}\oint_{C_0} Z'(\zeta)\frac{\mathrm{d}\zeta}{\zeta^n}, \quad n \geq 1. \tag{6.3}$$

Furthermore, $W_\Gamma(\zeta)$ now simplifies to

$$W_\Gamma(\zeta) = \frac{\mathrm{i}\Gamma}{2\pi}\log\zeta, \quad \zeta W_\Gamma'(\zeta) = \frac{\mathrm{i}\Gamma}{2\pi}. \tag{6.4a,b}$$

The time scale of the flow is fixed by setting $\Gamma = 2$ since we proceed on the assumption that this single-vortex configuration will connect in some way to the two-vortex configuration, each having circulation $\Gamma = 1$, studied previously. The condition on the vortex boundary is again given by (4.4)

$$\mathrm{i}\zeta H'(\zeta) = -q|Z'(\zeta)| + \Omega\overline{Z(\zeta)}\zeta Z'(\zeta) - \mathrm{i}\zeta W_\Gamma'(\zeta), \quad \zeta \in C_0. \tag{6.5}$$

The formulation again leads to two Schwarz problems for analytic functions in the unit disc, and since the unit disc is simply connected there are no longer any solvability conditions. We have

$$\mathrm{Re}[\zeta H'(\zeta)] = R_0(\zeta), \quad \zeta \in C_0, \tag{6.6}$$

with $R_0(\zeta)$ still given by formula (4.7) and this is a Schwarz problem in the disc for the analytic function $\zeta H'(\zeta)$. Its solution is furnished by the Poisson integral formula

$$\zeta H'(\zeta) = \frac{1}{2\pi\mathrm{i}}\oint_{C_0}\frac{\mathrm{d}\zeta'}{\zeta'}\left(\frac{\zeta'+\zeta}{\zeta'-\zeta}\right)R_0(\zeta') + \mathrm{i}c_1, \tag{6.7}$$

where the real constant $c_1 = 0$ in order to avoid $H(\zeta)$ having a logarithmic singularity at $\zeta = 0$. If we now define a modified function

$$F(\zeta) \equiv \log(\zeta Z'(\zeta)) + \log\zeta \tag{6.8}$$

then the logarithmic singularities of both functions at $\zeta = 0$ cancel out. Then

$$\mathrm{Re}[F(\zeta)] = \tilde{T}_0(\zeta), \quad \zeta \in C_0, \tag{6.9}$$

where

$$\tilde{T}_0(\zeta) \equiv \log(S_0(\zeta)) + \log|\zeta|. \tag{6.10}$$

This is the second Schwarz problem for the analytic function $F(\zeta)$ in the unit disc and the Poisson integral formula again provides the required solution.

The same iterative scheme as described in § 4.1 can now be deployed. In all results to follow the Laurent series (6.1) is truncated at $N = 32$ terms. Since the vortex centroid is expected to remain at the origin the length scale is now set by fixing the vortex area $\mathcal{A} = \pi$ with the vortex perimeter $\mathcal{P}$ now used as the continuation parameter starting from a circular vortex configuration of unit radius where

$$\mathcal{A} = \pi, \quad \mathcal{P} = 2\pi, \quad d = 1, \quad a_n = 0, \quad n = 1, \ldots, N. \tag{6.11a–d}$$

Since this circular configuration is degenerate – a circular vortex is an equilibrium for any values of q and Ω satisfying (2.10) – to bifurcate from this trivial branch it is necessary to seed the iteration with a non-zero initial value of a_1 which encodes elliptical distortions to

the circular vortex, that is, distortions with a 2-fold rotational symmetry about the origin. Indeed, a local analysis can be used to determine analytically the values of q and Ω at which steady solution branches with non-zero a_1 bifurcate from the circular solution. It can be posed that

$$Z(\zeta) = \mathrm{i}d\left[\frac{1}{\zeta} + \epsilon a_1\zeta + \ldots\right], \quad H(\zeta) = \epsilon h_2\zeta^2 + \ldots, \quad \epsilon \ll 1, \tag{6.12a,b}$$

where h_2 is the leading coefficient of $H(\zeta)$. These are the forms for an elliptical perturbation expected theoretically. These can be substituted into the boundary condition (6.5) which can then be linearised in ϵ. Both sides of this boundary condition can be expanded as a Laurent series convergent for $\zeta \in C_0$ and, on equating powers of ζ in these Laurent series, the conditions

$$\frac{\Gamma}{\pi} = dq + \Omega d^2, \quad \frac{q}{2} = d\Omega \tag{6.13a,b}$$

are deduced on equating the coefficients of ζ^0 and ζ^{-2} respectively. The first of these is just a restatement of condition (2.10). With $\Gamma = 2$ and $d = 1$ we can solve these two equations for q and Ω:

$$q = \frac{2}{3\pi}, \quad \Omega = \frac{1}{3\pi}. \tag{6.14a,b}$$

More generally, although we do not explore them here because they are tangential to our present goals, it is expected that there exist bifurcations, from a circular vortex, of steadily rotating hollow vortices with m-fold rotational symmetry about the origin of which the case of particular interest here is $m = 2$.

Figure 6 shows a graph of q and Ω against the rescaled perimeter $\mathcal{P}/2\pi$ for the family of single rotating hollow vortex solutions found using the numerical scheme. The two crosses shown on the graphs confirm that the numerical method retrieves the theoretical values (6.14*a*,*b*) just predicted and this provides a check on the numerical method.

The shapes of the hollow vortex for $\mathcal{P}/2\pi = 1.05$, 1.5 and 2.5 are shown in figure 7. As the perimeter increases the vortex is found to become elongated along the direction of the y-axis and eventually develop a 'waist' where the two sides of the vortex draw closer together. Eventually a limiting configuration at $\mathcal{P}/2\pi \approx 2.826$ is found where two distinct parts of the vortex boundary appear to almost touch; the calculations are terminated just before this occurs since such a touching configuration is not physically admissible. Figure 8 shows the (rescaled) near-critical configuration: two distinct parts of the vortex boundary are drawing close together and, as shown in the inset close-up, are separated by a distance of the order of 10^{-4}.

All the calculations point to the formation of what we refer to as a topological singularity: it is clear visually that the shape of the limiting configuration of the single rotating hollow vortex as its waist thins and the two sides of the vortex draw close together is very similar to the limiting configuration of the two rotating hollow vortices as the two 'fingers' protruding from each vortex nearly touch. Indeed, the calculations point to the two scenarios producing the same limiting shape, albeit via topologically distinct limits: compare figures 5 and 8 where the latter figure has been rescaled so that the vortex has the same area as the sum of the two vortices in figure 5. Quantitatively, if we introduce the length scale factor L based on the critical area $\mathcal{A}_{crit} = 0.311$ of each of the two corotating

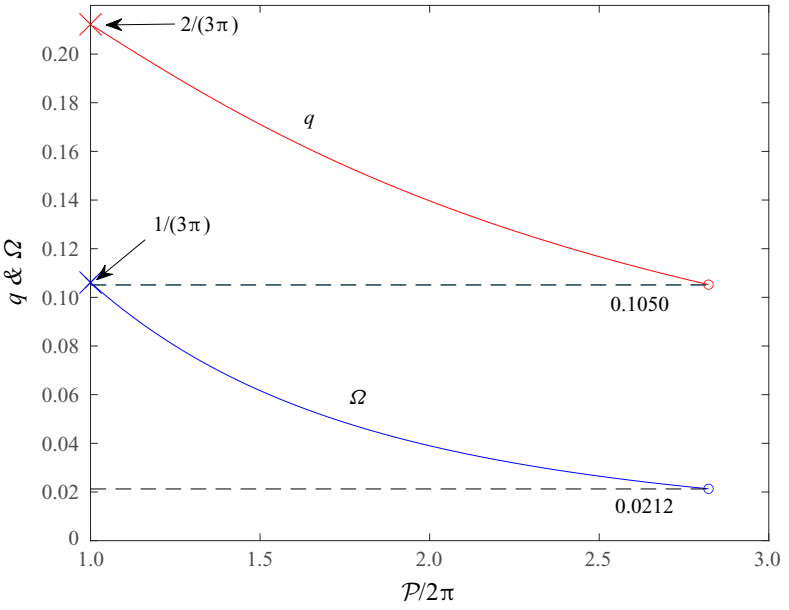

FIGURE 6. Graphs of q and Ω against $\mathcal{P}/2\pi$ for a single rotating hollow vortex. Values for the critical configuration are indicated by small circles. The q-curve intersects the axis at the cross at $1/(3\pi)$, the Ω-curve at the red cross at $2/(3\pi)$ as predicted in (6.14*a*,*b*).

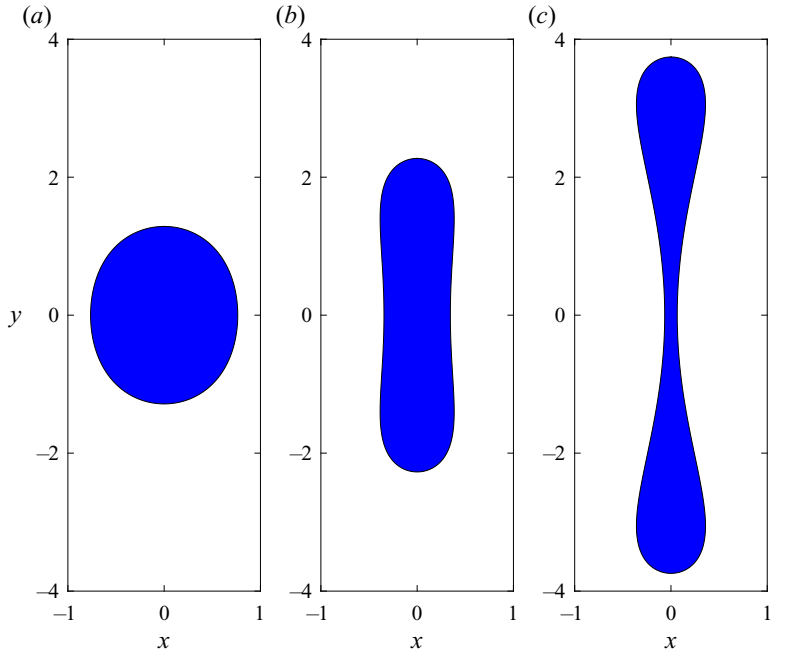

FIGURE 7. Typical equilibrium shapes of a single hollow vortex in the corotating frame for $\mathcal{P}/2\pi = 1.05$, 1.5 and 2.5. The vortices all have area $\mathcal{A} = \pi$. (*a*) $\mathcal{P}/2\pi = 1.05$; (*b*) $\mathcal{P}/2\pi = 1.5$; (*c*) $\mathcal{P}/2\pi = 2.5$.

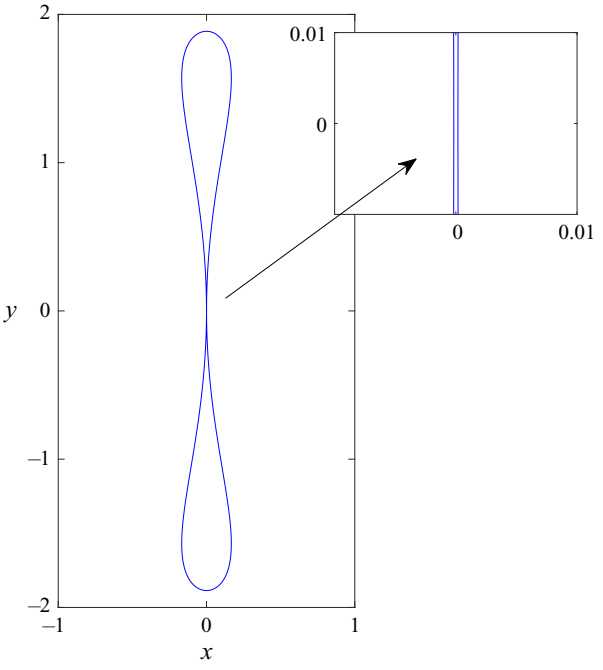

FIGURE 8. Near-critical shape of single rotating hollow vortex for $\mathcal{P}/2\pi = 2.826$ rescaled so that it has the same area as the two near-critical rotating hollow vortices of figure 5.

vortices shown in figure 2, namely,

$$L = \left(\frac{2 \times 0.311}{\pi}\right)^{1/2} \tag{6.15}$$

and use this to rescale the critical values of $q = 0.1050$ and $\Omega = 0.0212$ for the single vortex indicated in figure 6 we find

$$q^* = \frac{q}{L} = \frac{0.1050}{L} = 0.236, \quad 4\pi\Omega^* = 4\pi\left(\frac{\Omega}{L^2}\right) = 4\pi\left(\frac{0.0212}{L^2}\right) = 1.346, \tag{6.16a,b}$$

which are very close to the values indexed by daggers in table 1 and corresponding to the near-critical configuration of two hollow vortices shown in figure 5. We offer this as evidence that the single-vortex and two-vortex scenarios are tending to the same limiting configuration. The limiting 'touching' configuration itself is not physically admissible since, by the symmetry of the arrangement, the origin at which the vortices touch would need to be a stagnation point meaning that, for a continuous limit, we would need $q \to 0$. Figure 9 superposes a close-up of this topological transition based on the numerical calculations closest to transition calculated using both the single-vortex and two-vortex numerical codes.

7. Discussion

This paper, which is the first to study the notion of a 'rotating hollow vortex', has presented a study of a like-signed corotating vortex pair using the hollow vortex model. The nonlinear free boundary problem has been solved using a numerical method, suited to

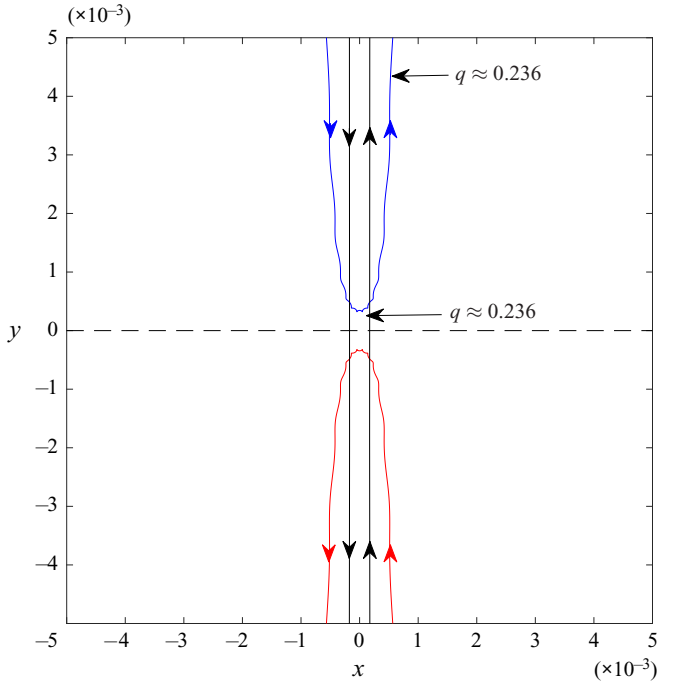

FIGURE 9. Illustration of the topological singularity: the topology of the vortex boundary changes but all physical quantities (q and Ω) are continuous across the singularity.

the doubly connected nature of the fluid domain, that captures almost the entire branch of solutions up to what we call a topological singularity where the two vortices are observed to form from the break-up of a single rotating hollow vortex and where all physical quantities are continuous across the transition. A family of corotating single-vortex structures has also been computed using a simple adaptation of the numerical scheme.

The results provide evidence of steady vortex merger: two rotating hollow vortices, starting as two distinct near-circular hollow vortices, are shown to deform through a continuous family of corotating equilibria to merge at a critical configuration to form a single rotating vortex structure; that single vortex is itself a continuous deformation from a single circular rotating hollow vortex. This is reminiscent of a similar result involving vortex patches found by Crowdy & Marshall (2004). Those authors also start with a corotating point-vortex pair and show, by growing two small vortex patches at the two stagnation points of the associated flow field in the corotating frame, that this 2-point-vortex equilibrium is connected to the circular Rankine vortex through the continuous family of non-trivial rotating equilibria involving the steady merger of the two vortex patches which eventually touch. This continuous sequence of equilibria is shown in figure 2 of Crowdy & Marshall (2004).

Conversely, the calculations show steady vortex break-up: a single rotating vortex forms a thin waist which touch at a critical angular velocity causing the vortex to break up into two distinct vortices. Based on the evidence here we conjecture that the recently computed single hollow vortex in shear (Zannetti *et al.* 2016), which also exhibits a limiting state with a thin waist, will similarly break up into two distinct vortex structures via a topological singularity of the kind exemplified here. The numerical algorithm presented here for the two-vortex case can be easily adapted to that scenario. Such steady pinch-off phenomena are characteristic of a single hollow vortex equilibrium in an irrotational straining flow

(Llewellyn Smith & Crowdy 2012) and we anticipate that similar topological singularities will be observed there too. It is also worth mentioning that a steady pinch-off akin to that observed here and in other hollow vortex problems is also observed in the different, but related, problem of a single non-rotating hollow vortex equilibrium with surface tension active on its boundary (Crowdy 1999; Wegmann & Crowdy 2000).

Steady vortex merger is, of course, quite different to dynamical merger and the related question of the stability of the equilibria found in this paper remains to be investigated. Stability studies on hollow vortex equilibria are still rare, with the linear stability of Pocklington's (1895) cotravelling vortex pair only studied recently by Crowdy *et al.* (2013). The stability of an isolated hollow vortex in strain was studied by Llewellyn Smith & Crowdy (2012) around the same time. As mentioned in the Introduction, the idea of using the non-existence of steady equilibria as a signature of dynamical vortex merger is well known (Meunier *et al.* 2002; Leweke *et al.* 2016) and, for this, the maximum area solution found here might have some relevance. For the rotating hollow vortex pair, however, it is interesting to note that it is not true that the diagnostic a/b put forward by Meunier *et al.* (2002) reaches a maximum value before the critical state is reached. Indeed, we have found that $a/b = 0.260$ at the maximum area configuration but continues to increase to $a/b = 0.283$ close to the topological singularity. This is believed to be due to the peculiarity of the hollow vortex model in having a good portion of its total net circulation carried in its boundary.

The formulation here should be straightforward to extend to $N > 2$ rotating hollow vortices in a polygonal ring thereby extending the classic study of Thomson (Saffman 1992) to rotating polygonal rings of hollow vortices. A direct extension of the approach herein would use prime functions associated with higher connected domains (Crowdy 2020); in terms of those functions there exist convenient integral formulas for solutions to the modified Schwarz problems that would generalise those arising here. Moreover, the same calculus given by Crowdy (2010) would provide the relevant $W_\Gamma(\zeta)$ function generalising that used in (3.6). It would be interesting to see if similar topological singularities exist between limits of those N-vortex solutions and limiting states of higher-order N-fold symmetric bifurcations from a single circular hollow vortex.

The solutions here sit within a broader class of vortex structures of 'Sadovskii type' (Sadovskii 1971; Saffman 1992); these are vortex patches with vortex sheets on their boundaries (rather than just vortex jumps). A recent study of such structures in ambient flow fields has been carried out by Freilich & Llewellyn Smith (2017) where a parameter is introduced that governs the amount of the total vorticity of the structure that is held in the patch compared to the boundary sheet. In the solutions considered here this parameter has been set implicitly by insisting that the fluid inside the hollow vortices is in pure solid body rotation which slaves the choice of this patch vorticity to the angular velocity of the combined structure. However, this condition can presumably be relaxed and broader classes of 'steadily rotating Sadovskii vortex pairs' are expected to be available.

Acknowledgements

R.B.N. and D.G.C. received support from the Engineering and Physical Sciences Research Council (EP/K019430/10). D.G.C. acknowledges a Royal Society Wolfson Research Merit Award. V.S.K. acknowledges financial support from CAPES/Brazil through a Science Without Borders postdoctoral program during his stay at the Federal University of Pernambuco, Recife. All authors acknowledge support from EPSRC grant EP/R014604/1 during the 'Complex analysis: techniques, applications and computations' program at the Newton Institute in Cambridge (Sep-Dec 2019).

Declaration of interests

The authors report no conflict of interest.

REFERENCES

BAKER, G. R., SAFFMAN, P. G. & SHEFFIELD, J. S. 1976 Structure of a linear array of hollow vortices of finite cross-section. *J. Fluid Mech.* **74**, 469–476.

BATCHELOR, G. K. 2000 *An Introduction to Fluid Dynamics*. Cambridge University Press.

CROWDY, D. G. 1999 Circulation-induced shape deformations of drops and bubbles: exact two-dimensional models. *Phys. Fluids* **11** (10), 2836–2845.

CROWDY, D. G. 2008 The Schwarz problem in multiply connected domains and the Schottky-Klein prime function. *Complex Var. Elliptic* **53**, 221–236.

CROWDY, D. G. 2010 A new calculus for two-dimensional vortex dynamics. *Theor. Comput. Fluid Dyn.* **24**, 9–24.

CROWDY, D. G. 2020 *Solving Problems in Multiply Connected Domains*. Society for Industrial and Applied Mathematics.

CROWDY, D. G. & GREEN, C. C. 2011 Analytical solutions for von Kármán streets of hollow vortices. *Phys. Fluids* **23**, 126602.

CROWDY, D. G. & KRISHNAMURTHY, V. S. 2018 The effect of core size on the speed of compressible hollow vortex streets. *J. Fluid Mech.* **836**, 797–827.

CROWDY, D. G. & MARSHALL, J. S. 2004 Growing vortex patches. *Phys. Fluids* **16**, 3122–3129.

CROWDY, D. G., LLEWELLYN SMITH, S. G. & FREILICH, D. V. 2013 Translating hollow vortex pairs. *Eur. J. Mech.* B/*Fluids* **37**, 180–186.

DRITSCHEL, D. G. 1985 The stability and energetics of corotating uniform vortices. *J. Fluid Mech.* **157**, 95–134.

FREILICH, D. V. & LLEWELLYN SMITH, S. G. 2017 The Sadovskii vortex in strain. *J. Fluid Mech.* **825**, 479–501.

LEWEKE, T., DIZÉS, S. L. & WILLIAMSON, C. H. K. 2016 Dynamics and instabilities of vortex pairs. *Annu. Rev. Fluid Mech.* **48**, 507–541.

LLEWELLYN SMITH, S. G. & CROWDY, D. G. 2012 Structure and stability of hollow vortex equilibria. *J. Fluid Mech.* **691**, 178–200.

MELANDER, M. V., ZABUSKY, N. J. & MCWILLIAMS, J. C. 1988 Symmetric vortex merger in two dimensions: causes and conditions. *J. Fluid Mech.* **195**, 303–340.

MEUNIER, P., EHRENSTEIN, U., LEWEKE, T. & ROSSI, M. 2002 A merging criterion for two-dimensional co-rotating vortices. *Phys. Fluids* **14**, 2757–2766.

POCKLINGTON, H. C. 1895 The configuration of a pair of equal and opposite hollow straight vortices of finite cross-section, moving steadily through fluid. *Proc. Camb. Phil. Soc.* **8**, 178–187.

SADOVSKII, V. S. 1971 Vortex regions in a potential stream with a jump of Bernoulli's constant at the boundary. *Z. Angew. Math. Mech.* **809**, 729–735.

SAFFMAN, P. G. 1992 *Vortex Dynamics*. Cambridge University Press.

SAFFMAN, P. G. & SCHATZMAN, J. C. 1981 Properties of a vortex street of finite vortices. *SIAM J. Sci. Stat. Comput.* **2** (3), 285–295.

SAFFMAN, P. G. & SZETO, R. 1980 Equilibrium shapes of a pair of equal uniform vortices. *Phys. Fluids* **23**, 2339–2342.

TANVEER, S. 1986 A steadily translating pair of equal and opposite vortices with vortex sheets on their boundaries. *Stud. Appl. Maths* **74**, 139–154.

TELIB, H. & ZANNETTI, L. 2011 Hollow wakes past arbitrarily shaped obstacles. *J. Fluid Mech.* **669**, 214–224.

WEGMANN, R. & CROWDY, D. G. 2000 Shapes of two-dimensional bubbles deformed by circulation. *Nonlinearity* **13**, 2131–2141.

ZANNETTI, L., FERLAUTO, M. & LLEWELLYN SMITH, S. G. 2016 Hollow vortices in shear. *J. Fluid Mech.* **809**, 705–715.